NSF GRANT #0755995
NSF PROGRAM NAME: NANOMANUFACTURING

Gas Phase Nanoxerographic Nanomaterial Integration

Lead P.I. Heiko O. Jacobs*
University of Minnesota - Electrical Engineering

Jesse Cole, En-Chiang Lin, Jun Fang, and Forrest Johnson
University of Minnesota - Electrical Engineering

Abstract: This technical paper reports progress on two fronts on the proposed research in the field of Nanoxerography.

Aspect 1 reports on a new nanolens approach on the basis of charged resist structures to print nanoparticles with high resolution – a 3 fold size reduction has been observed between the structures and the assembled particles. Directed assembly was observed due to a naturally occurring inbuilt charge differential at the material interface which was further enhanced by corona charging to yield a field strength exceeding 1 MV/m in Kelvin Probe Force Microscopy (KFM) measurements. The assembly process is independent of the nanomaterial source and type – an evaporative, plasma, and electrospray source have been tested to deposit silicon and metallic nanoparticles.

Aspect 2 reports on a new approach to produce high resolution charge patterns using a process that can be scaled to large areas since prior processes were limited to cm^2 sized substrates. A new process was discovered that can potentially scale Nanoxerography to large area printing and possibly roll-to-roll processing. While an extension to roll-to-roll is outside of the scope of the proposed work we decided to include preliminary results on the process in this report. The process is called Nanocontact Electrification and uses forced de-lamination of insulating surfaces which result in uncompensated surface charges. The process produces charged surfaces and associated fields that exceed the breakdown strength of air leading to strong long range adhesive forces and force distance curves which are recorded over macroscopic distances. The process is applied to fabricate charge patterned surfaces for nanoxerography demonstrating 200nm resolution nanoparticle prints and applied to thin film electronics where the patterned charges are used to shift the threshold voltages of underlying transistors.

Aspect 1: Nanoxerography Exploring Fringing Fields and Electrodynamic Nanolens

1.1 Introduction: The ability to print, deposit, or assemble nanomaterials in two and three dimensions will enable the fabrication of a whole range of novel devices. There is a distinction to be made between the first generation devices that are formed by patterning films and nanomaterials using conventional lift-off and etching techniques and the second generation devices that require a localized order, placement, and formation of interconnects on a single nano-component (nanoparticle or nanowire) basis. Current examples of the second generation devices that require interconnects and/or localized order of single components include single nanocomponent transistors[1-3], light emitting diodes, lasers[4], sensors[5], passive photonic networks[6], or nanoparticle based media for data storage[7]. New technologies that can deliver and integrate single components at precise addressable locations on a surface are needed to enable the manufacturing of the second generation devices. Most recent research has focus on concepts that are based on directed self-assembly and template assisted assembly[8,9], exploring a variety of different forces including hydrophobicity / hydrophilicity[10], magnetic interactions[11], electro-spinning[12], microfluidics[13], and electrostatics or coulomb forces[14-21]. Interestingly most of these concepts, except those using electrostatics[14-18] and electrospinning[12], are exclusive to the assembly from the liquid phase. Liquid phase concepts considering solution chemistry as the nanomaterial source are important; however, an equally large amount of functional nanomaterials are formed using gas phase methods. The semiconductor industry for example uses gas-phase synthesis and deposition techniques exclusively when high-performance materials (conductors, semiconductors, and insulators) are needed. While the materials are often considered to be of better quality there are a number of limitations: patterning by etching and lift-off wastes materials, the resolution is limited by the resist pattern, and

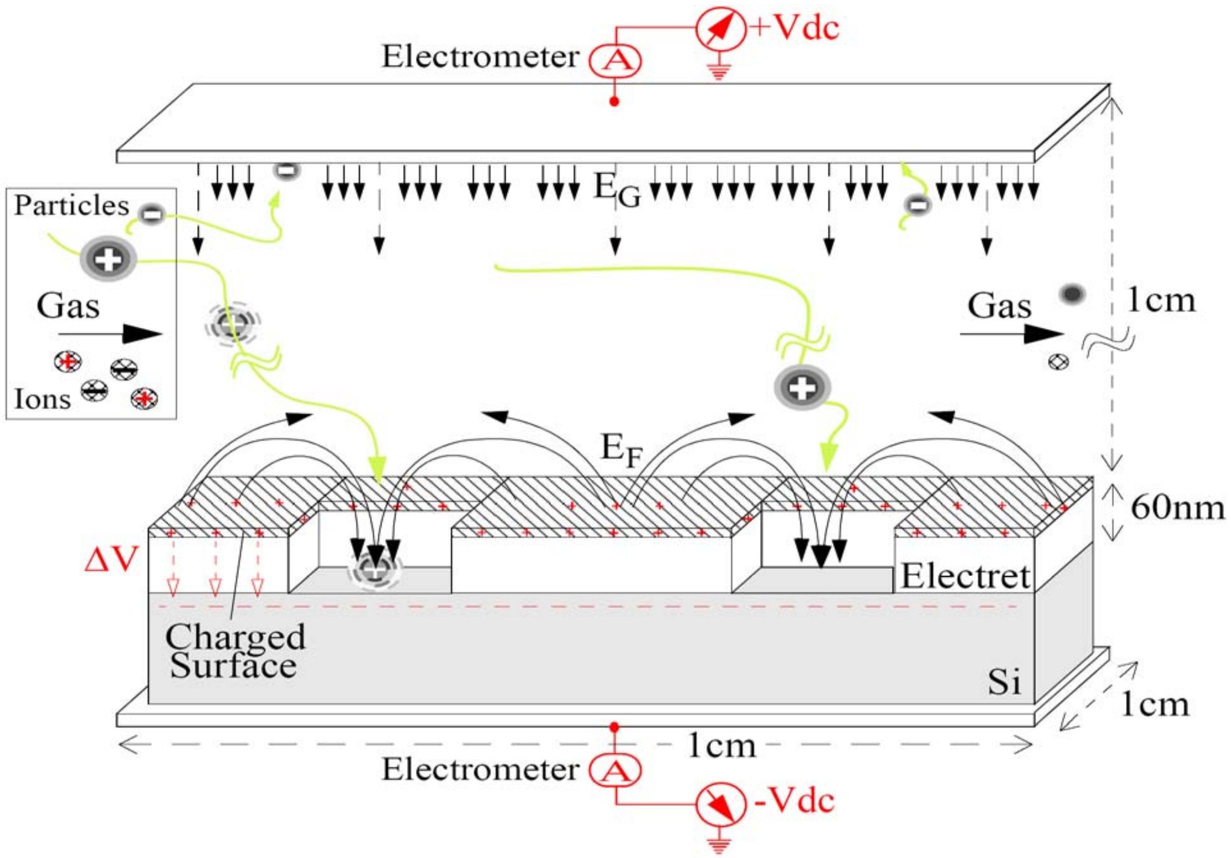

Figure 1.1 Illustration of the sample and assembly module. A carrier gas delivers charged nanoparticles and ions. A global field E_G directs charged particles of selected polarity towards the charged sample surface establishing an electrometer current. A potential ΔV is present between the electret and substrate. The potential gives rise to local fringing fields E_F that direct nanoparticles into the openings. As electrets we used SiO_2 or PMMA resist patterns with openings to a Si substrate. The patterns can be generated by any number of lithography methods. In our experiments we used standard photolithography for large scale features (>10 µm) and electron beam (e-beam) or nanoimprint lithography for small scale features (< 1 µm). The large scale features were 15 µm square holes in 100 nm thick thermally grown silicon dioxide on a p-type silicon substrate. The holes were formed by standard lithography and reactive ion etching and not treated any further. The high resolution samples consisted of 100 nm – 1µm wide holes and lines in a 60-80 nm thick layer of PMMA (2% 950K in Chlorobenzene) that was spin coated onto a n-type silicon wafer. The patterns were defined using electron beam lithography and developed in a 3:1 solution of IPA (isopropyl alcohol): MIBK (methyl isobutyl ketone) for 40 seconds.

randomness is observed in the deposition patterns if discrete nanoparticles or nanowires are deposited.

This communication presents a new directed assembly process that can be attached in a modular form to existing[14,16,22,23] gas phase systems. The approach is different from prior nanoxerographic printing methods that use continuous dielectric film layers. The primary aim of the approach is to direct single nanoparticles into addressable regions on a surface with sub-100 nm control over the position. It is an additive process that directs the material into target locations, conserving material and eliminating lift-off or etching steps. The process works at atmospheric pressure and intermediate vacuum (10^{-4} torr) and employs a carrier gas that transports charged nanomaterials from a reactor into an assembly module. It combines Coulomb force directed assembly[16-18] with topographically patterned materials that can be formed by conventional lithography.

1.2. System Design: Figure 1.1 illustrates the gas-phase nanomaterial deposition concept. A global (E_G) and localized (E_F) electrostatic fringing field is used to direct the assembly of charged nanomaterials into micro or nanometer sized openings. The assembly occurs inside a 1 cm tall insulating channel with inlet and outlet on either side that holds two 1cm x 1cm squared top and bottom copper electrodes. The fringing field is formed using a charged, patterned thin film on top of a silicon chip. The surface of the electret is at a different electrostatic potential than the silicon chip. Electrostatic field lines are present not only inside the electret but also outside, affecting the nanoparticle trajectories. The line integral $\int \boldsymbol{E_F} d\boldsymbol{l} = \Delta V$ relates the strength of the fringing field (E_F) with the potential difference (ΔV) between the charged electret surface and the substrate. The externally biased electrodes select and direct incoming particles of a desired polarity towards the chip surface. Both electrodes are connected to an electrometer (Keithley 6517A) to monitor the current and charge that arises when charged nanomaterials or ions deposit on the surface. In this Faraday cup arrangement, image charges flow from the ground through the electrometer into the sample or electrode plate to the location of assembled material. As a result, the electrometer measures the accumulated charge and subsequent current of the assembled particles or ions regardless of where they deposit on the surface or whether they become neutralized by the image charges. The deposition rate onto the plates inside this assembly module depends on the volume number concentration of charged nanomaterials and ions, gas flow, actual potential difference between the two plates, and pressure. It can be adjusted ranging from 3 pA at ultra low concentrations to 1 nA at high concentration.

As a nanoparticle source we have tested three different systems, an evaporative[16], electrospray[22], and plasma[23] system, to create metallic and semiconducting nanoparticles (10-50 nm in size). The evaporative and electrospray system outlets are connected to the assembly module through a 1 cm diameter, 15-20 cm long Tygon tube. A mixture of CO_2 and compressed air with flow rates of 300 and 800 sccm, respectively, are used as carrier gases in the electrospray system to transport the nanomaterials into the assembly module. A 1500 sccm flow of argon is used in the evaporative system.

Both SiO_2 and PMMA on silicon exhibited an inherent built-in potential ΔV that can be changed by additional surface treatments. The potential ΔV that gives rise to the fringing fields is the key parameter in the self-assembly process. We have directly measured these potentials as a function of processing conditions using Kelvin Probe Force Microscopy (KFM)[24]. KFM is an atomic force microscopy based tool that can detect variations in the surface potential distribution with 100 nm scale lateral resolution and 5 mV sensitivity. Figure 1.2 illustrates an example of the change in surface potential difference between PMMA thin films and exposed silicon areas after different processing steps: (a) electron beam lithography and (b) corona charging. Figure 1.2a shows a 60 nm thick PMMA film on top of an n-type silicon wafer with a native oxide after e-beam exposure, development in MIBK, rinsing in IPA, and blow drying under a stream of dry nitrogen. The film contains 100 nm diameter holes and a 500 mV potential difference. As a qualitative statement, we rarely observed charge or potential differentials between dissimilar surface regions that are zero. The observation of a charge differential is the norm rather than the exception and has been used as a material contrast mechanism since 1997.[25] The charge differential between the patterned PMMA thin films and the underlying native oxide varied with the processing conditions. Silicon without native oxide did not show a strong charge differential (recorded values were smaller than 100 mV) which leads to the conclusion that the native oxide plays an important role. Our current hypothesis is that the PMMA is highly negatively charged during e-beam exposure yielding a positive image charge in the silicon and native oxide layer underneath that could remain partially present after developing the PMMA in MIBK. We were able to remove >90% of the charge by dipping the chip in a 2% solution of HF in water for 30 seconds which supports this hypothesis. However, other mechanisms such as charging by contact and friction when rinsing the dissimilar surfaces (PMMA and native silicon) with MIBK, IPA, and blow drying under a stream of dry nitrogen cannot currently be excluded.

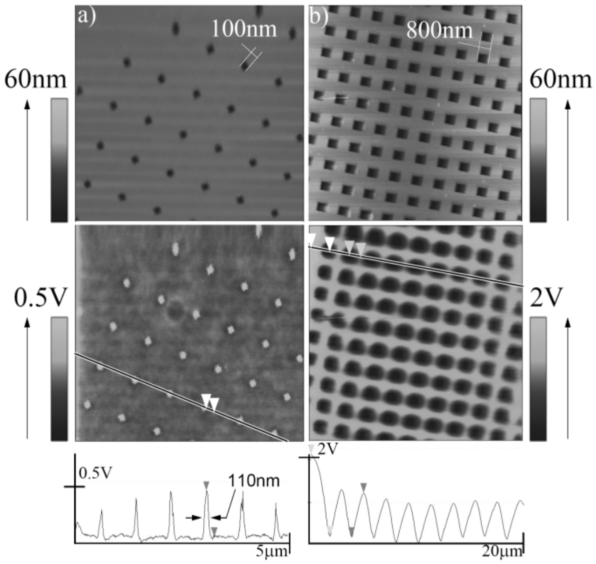

Figure 1.2. (top) Atomic force microscopy topographical images of the nanostructured PMMA and (bottom) corresponding surface potential images. a) Sample charged during the electron beam lithography process. b) Corona charged sample.

Moreover the recorded potential difference can be reversed or enhanced by a number of different methods including a previously published concept[15,16] in which externally biased conformal electrodes are used to establish an electrical contact with the electret surface to reverse the potential. We tested this approach and obtained a potential difference of 500 mV for the 60-80 nm thick PMMA film. These potentials show greater stability suggesting that the charge is embedded inside the PMMA film.

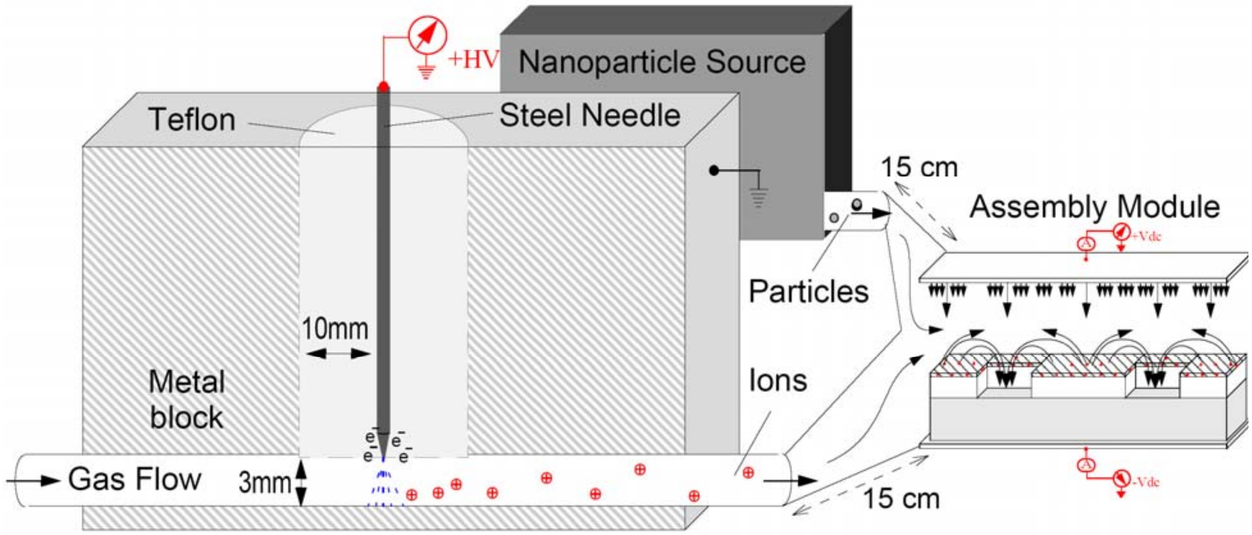

Figure 1.3. Inline corona charger. A high voltage is applied to an insulated needle positioned 3mm away from a grounded metal tube. The induced electric field creates a corona region where ions are repelled from the needle and carried away by the carrier gas to the assembly module.

1.3. Charging Technique: Figure 1.3 shows a new charging method that was used to create the 2V potential difference in Figure 1.2b. The approach combines patterned electrets on conducting substrates with corona charging. A homebuilt corona charger – loosely based on work by Whitby et al.[26,27] – was used and connected to the particle assembly module. Argon gas was flown (1000 sccm) through the charger and ionized using a positive DC corona discharge by applying a positive (2.5kV) potential between the stainless steel needle and metal encasement. A fraction of the argon ions are carried away by the gas flow into the assembly module. We measured these ions inside the assembly module using the electrometer which recorded negative 48 nC of accumulated charge on the positively biased (100 V) top plate and a positive 360 nC of charge on the negatively biased (-100 V) bottom plate after 20 minutes of charging. A partial amount of the positive Ar ions are trapped on or inside the insulating electret surface whereas the conducting silicon surface remains less affected. This approach was very successful; it yielded high potential differences exceeding 2V (fig. 1.2b) between the nanostructured PMMA layer and semiconducting substrate. The observed 2V potential difference for the corona charged samples exceeds to the best of our knowledge any previously reported values for PMMA thin films of similar thickness. We attribute the broadening in the highly corona charged samples to be dominated by repulsive Coulomb forces and charge diffusion instead of tip related convolution. The charge retention time varied greatly with electret material, charging method, humidity, and storage container. Qualitatively, thermally grown silicon oxide did not retain its charge as well as PMMA and frequently lost most of its charge within less than 5 hours. Electric contact charged PMMA yielded superior retention times but lower charge differentials than corona charged samples. All electrets (SiO_2 and PMMA), independent of the charging methods, retained a sufficiently large charge differential to conduct successful assembly experiments for several hours.

1.4. Nanoparticle Assembly Results: Figure 1.4 shows the first assembly attempt using a 30 µm pitch that illustrates the importance on balancing the strength of global and local fields. In theory perfect assembly could be accomplished without any particles depositing on the resist structures if the local fields are strong and the global field is zero. The assembly would be largely independent of the pitch or layout of the pattern. The problem, however, is that the assembly process would not proceed very fast; a small global field is needed to direct nanomaterials to the surface and the superposition of the two contributions has to be considered. Particles can and will end up in undesired areas on the resist structures if the empty areas exceed a certain threshold. In the illustrated experiment we used a patterned SiO_2 substrate positively charged by electric contact charging with a flat gold coated PDMS stamp.[15] The surface potential difference was measured by KFM to be ΔV=300 mV. A global electric field strength E_G of 20kV/m (+200V top electrode, -200V bottom electrode) was used to initially direct the incoming particles.

The field on the silicon dioxide surface can be approximated to be $E_s = \Delta V/(\pi r) - E_G$ considering simple parallel lines and half circular field lines with radius r. This is a crude estimate which is only valid for a single step potential but it provides important insights into the basic principle. For example it allows us to calculate a

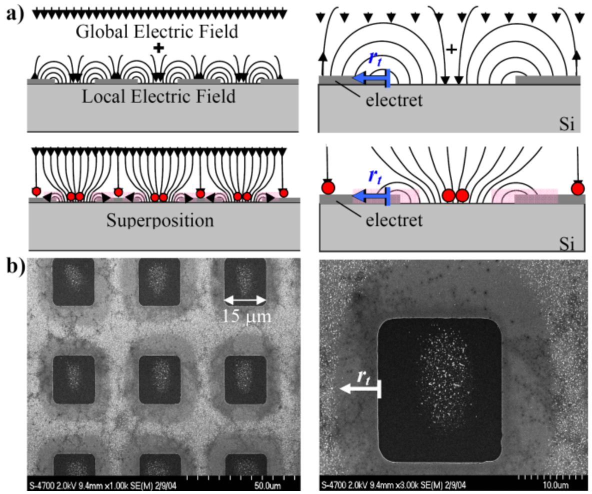

Figure 1.4. (a) Conceptual picture and (b) experimental result illustrating the effect of the global potential on the size of the empty areas. A 10 µm wide empty belt is visible. Holes are 15µm wide.

turning point $r_t = \Delta V/(\pi E_G)$ where the local field on the PMMA surface is equal to the global field. Beyond this turning point particles will deposit on top of the resist structures. In the given case, the calculated value for r_t is ~5 µm; the actual experimental values ranged from 5 to 7 µm. Another distinctive element is that the 15 µm openings are partially empty resulting in focused assembly towards the center. The positively charged gold nanoparticles shown in Figure 1.4 were 10-100 nm in size and generated by evaporation, nucleation, and condensation within a tube furnace and carried to the particle assembly module in a 1.5 liter/minute flow of argon.[16]

Figure 1.5 shows high resolution patterns where the focusing effect becomes much more prevalent. The pitch has been reduced when compared to Figure 1.4. As long as r_t is larger than the actual pitch of the patterns we find no particles on the PMMA coated areas. The openings create attractive funnels for particles to assemble into the holes which are largely independent of the pitch. Figures 1.5a and 1.5b depict 10-40 nm silver nanoparticles created in the evaporative furnace system and assembled into ~100nm sized holes in corona charged PMMA. By analyzing 130 holes we derived the standard deviation from the center location to be ~25 nm. The assembly parameters were as follows: 1500 sccm argon gas, atmospheric pressure, 1080 °C furnace temperature, 200 V global applied potential, 3 nC recorded charge accumulation, and 10 minute assembly duration. Figure 1.5c shows gold colloids that have been assembled into the center of 300 nm wide trenches. A full width at half maximum resolution of ~75 nm was found by analyzing the 770 particles assembled in the three central lines of figure 1.5c. The gold colloids were assembled using an

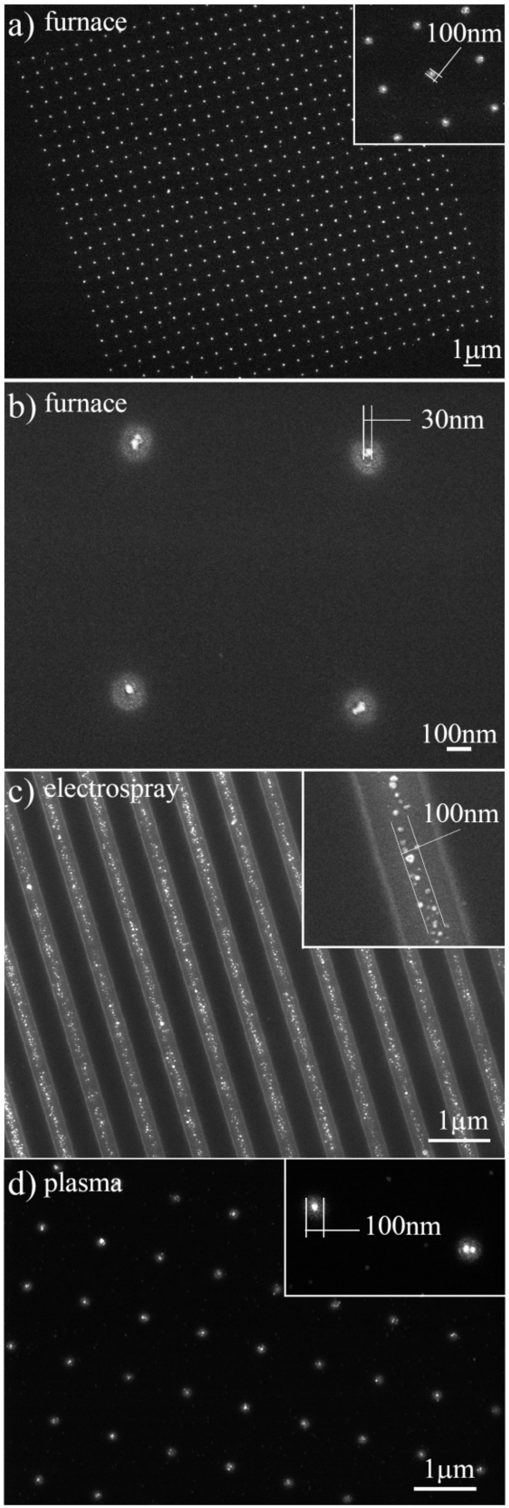

Figure 1.5. Nanoparticle assembly into holes and lines. a,b) Silver nanoparticles focused into the center of ~100nm holes from the evaporative furnace system. c) 50nm colloidal gold particles focused along the central area of 300 nm wide lines from the electrospray system. d) 40nm cubic silicon particles assembled into 100nm holes from a capacitively coupled plasma system.

electrospray system[22] that has been published previously. A 14µM suspension of 50nm colloidal gold particles in water (BBInternational) was electrosprayed as received from the manufacturer without any alterations. The experimental parameters were as follows: a mixture of 300 sccm CO_2 and 800 sccm compressed air carrier gas, atmospheric pressure, ~100 nA electrospray current, 200 V global applied potential, 270 nC recorded charge accumulation, and 1.5 hr. assembly duration. The longer assembly time for this process can be attributed to low solution concentration and low charge concentration on the particles due to the presence of a Polonium 210 neutralizer[22]. Figure 1.5d shows 40 nm silicon nanoparticles that have been created in a constricted, filamentary, capacitively-coupled, low-pressure plasma system[23]. Particles in this system are charged and we were able to extract them from the flow. There is ~ 6 orders of magnitude lower pressure in this system than in the evaporation and electrospray system. While we have been able to assemble the particles, the repeatability is not as consistent when compared to systems that deliver particles at atmospheric pressure. The primary reason points to a specific design problem. The plasma generated particles enter a lower pressure chamber at high speeds (50 – 70 m/s)[28] and reach a nanoparticle assembly module with greater variations in the kinetic energy distribution. The estimated retained energy is at least one order of magnitude higher than the thermal energy in an atmospheric pressure system.

Figure 1.6 depicts representative electron micrographs of gold nanoparticles that are deposited onto a silicon substrate electrode that was partially shielded using a 80 nm thick e-beam patterned PMMA layer (A,B) and 500 nm thick Shipley 1805 photoresist (C,D,E,F). The text structure (A) and interconnected square structures (B) were developed in 120 seconds which illustrates that the gold nanoparticles can be focused with sub 100 nm lateral resolution without finding any particles on the resist itself. This is quite remarkable. The insulating surfaces appear to self-equilibrate to a sufficiently high potential for the nanoparticle flux to be directed to the grounded regions. The focusing effect and the small standard deviation in the location of the deposits become apparent using 1 µm circular openings (C,D,E). Here the particles initially deposit into an area that is approximately 7 times smaller than the opening but spread out over time yielding tower like structures that can be several micrometers tall (D). Continued deposition causes the tops of towers to broaden (E). These towers contain several hundred layers of 10-20 nm particles. Thin < 1µm deposits (A,B) are very uniform over large areas while thick >2µm deposits (F) begin to show some level of variations over mm sized areas.

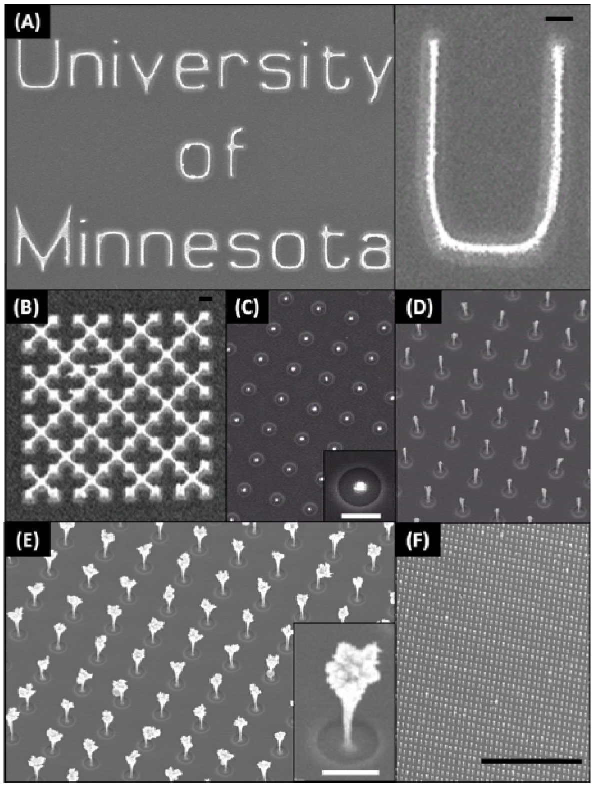

Figure 1.6. Representative images of nanoparticle deposits limited to Au as a function of deposition time increasing from 2 minutes (A,B,C) to 15 minutes (D) to 30 minutes (E,F) at constant 10W arc discharge power. Particles deposit into openings in 80nm thin PMMA ebeam resist (A,B) or 0.5µm thick Shipley 1805 photoresist (D,E,F) with a minimal lateral resolution of 60 nm. Particles do not deposit on the resist. Scale bars: 100nm in (A inset), 1 µm in (B), 1 µm in (C, E insets), and 100 µm in (F).

In conclusion, we have developed a new gas-phase integration process to assemble nanomaterials into desired areas using localized fringing fields. We expect this process to work with any material that can be charged including organic and inorganic, metallic, semiconducting, and insulating materials. An interesting focusing effect has been observed that shows assembly at a resolution greater than the underlying pattern. The lateral placement accuracy – currently 25nm standard deviation for the evaporation system – is defined by the level of control of the focusing effect as well as the minimal feature size of the underlying patterns, presently 100 nm. The resist does not carry particles in a belt surrounding the patterns. The size of the empty resist areas depends on the ratio between local and global field strength and has been larger than 10 µm. The process offers self-aligned integration and could be applied to integrate single crystal silicon nanoparticle transistors[2] or other nanomaterial devices on desired areas on a surface. It could also be extended to externally biased surface electrodes that could be programmed to enable the integration of more than one material type.

Aspect 2: Nanoxerography by Nanocontact Electrification

2.1 Introduction: Prior processes to produce high resolution charge patterns that enabled nanoxerography with sub 100 nm lateral resolution used serial scanning probes and parallel electric nanocontact printing[29,30]. Both techniques use an intimate electrical contact to locally inject charge into thin film electrets and require the application of an external voltage to a conducting substrate. While they enabled the invention of Nanoxerography they have remained limited to small area patterning mainly because of the difficulty to get uniform electrical charge injection over large areas exceeding cm^2 sized substrates. Research Aspect 2 investigates a new potential solution that eliminates the requirement to use an electrical contact and external voltage to inject charge into a dielectric thin film. The approach explores the use of contact electrification. Contact electrification is a well known phenomenon which can be attributed to three fundamental processes; transfer of electrons, ions, or charged material. Contact electrification leads to uncompensated surface charges that significantly impact the force of adhesion. These forces can be very large. Measurements using point contacts between crossed cylinders recorded record levels where the electrostatic forces exceeded 6 joules per m^2 which is in the range of fracture energies for covalently bonded materials.[31] Considering the context of soft-lithography,[32] nanoimprint lithography, and nanotransfer printing,[33] the formation and fracture of conformal contacts have become mainstream and are no longer limited to single point contacts between crossed cylinders. Many techniques currently exist for the patterning of charges on a surface including direct writing[19] charges by AFM, parallel patterning[34] by contact with a thin flexible gold electrode, exposure to electron[21] and ion[35] beams, applying the photovoltaic[36] effect, and jet printing[37] of a charged solvent. The applications for these charged surfaces have been directed primarily towards the assembly of oppositely charged nanoparticles from the gas and liquid phases. When immobilized in a predetermined location nanoparticles could form the building blocks of next generation nanoelectronic devices that take advantage of nanoparticle properties including high crystallinity and large surface area. This motivates a new set of investigations into the fundamental science and applications of contact electrification at these interfaces over extended surfaces using multiple contacts of different size and shape.

This article reports a first set of experiments and results of high levels of contact electrification which occurs between poly(dimethylsiloxane) (PDMS) stamps that are brought in contact with silicon dioxide (SiO_2) and poly(methyl methacrylate) (PMMA). The experiments yield charged surfaces and associated fields that exceed the breakdown strength of air leading to strong long range adhesive forces. Proton exchange reactions established in solution chemistry are proposed to explain the observed interfacial charging. The process finds several applications. It is applied to the printing of charge, printing of nanoparticles, and charge based doping to shift the threshold voltage of thin film transistors. Regarding the charge patterning application, the chemically driven process eliminates the need for prior[34,38-40] conducting electrodes and external voltages to deliver and pattern charge. The charge patterns attract nanoparticles and support ~100 nm resolution prints containing <50nm Ag particles. Finally, in the context of printable electronics it is demonstrated that a contact with PDMS leads to high levels of uncompensated surface charge which affects transport in nearby semiconducting device layers which is measured in terms of transistor threshold voltage shifts which exceeded 500mV in the MOSFET devices that have been tested.

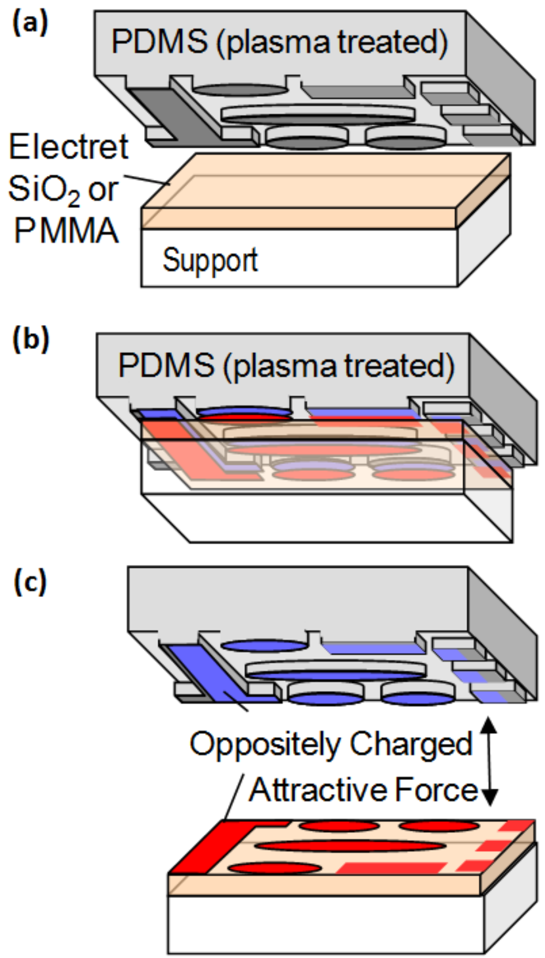

Figure 2.1. Contact electrification process. (a) A dielectric coated substrate is placed in contact with an oxygen plasma treated, patterned PDMS stamp. (b) Charge transfer occurs at the areas of contact between both materials and leads to an increase in short range adhesion. (c) Forced delamination yields oppositely charged surfaces and long range attractive force.

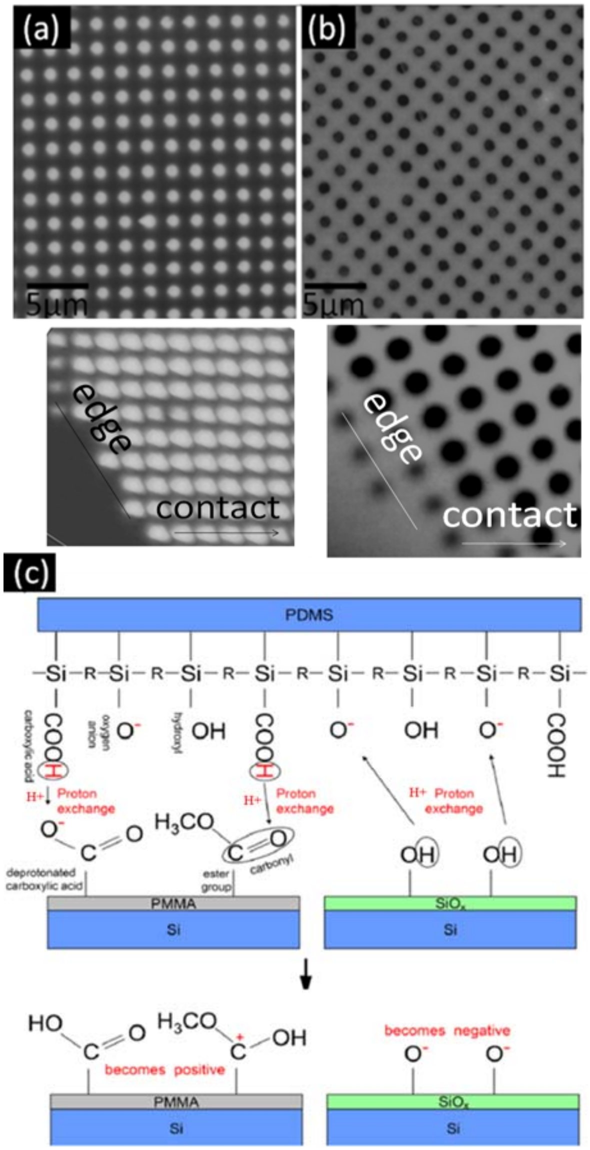

Figure 2.2. KFM contact electrification results and charge transfer theory. (a,b) KFM images of 1 µm pitched dot patterns showing the influence of material on the polarity. (a) PMMA charged positively and (b) SiO_2 charged negatively upon contact with the same plasma activated PDMS stamp. The edge of stamp-contacted region was recorded to determine the extent of lateral charge diffusion. (c) Proposed proton exchange reaction. In the case of PMMA, hydrogen protons dissociate from the PDMS surface and attach to a deprotonated carboxylic acid or carbonyl site within the ester groups on the PMMA surface. The situation is reversed for SiO_2 due to the abundance of hydroxyl groups on the SiO_2 surface.

2.2 Charging Process: Figure 2.1 illustrates the nanocontact electrification process between insulating surfaces. PDMS was chosen as the primary contacting material and was either patterned in topography through molding[34,38] to provide small contact areas surrounded by unchanged surface areas or it was left flat to lay down a uniform layer of charge. To clean and activate the PDMS surface (Figure 2.1a) we used a pure oxygen plasma etcher (SPI Plasma Prep II) operating at 80-100 watts at 10 Torr for 40 seconds. This process is used because it creates an energetic, hydrophilic surface that reduces transfer of uncured material during contact when compared to untreated PDMS.[41-44] Untreated PDMS did not result in high levels of charge transfer. As electrets we tested PMMA and SiO_2. The PMMA was spin-coated and baked according to standard procedures to produce a film thickness of 200 nm. The SiO_2 layer was a 160 nm thick and was generated by dry thermal oxidation. The nanocontact electrification process involves bringing the two dielectric surfaces in conformal contact (Figure 2.1b), leaving the surface in contact to react for 1 minute, and delamination. The delamination process (Figure 2.1c) yields oppositely charged surfaces patterns on each side which are characterized using Kelvin Probe Force Microscopy (KFM).[45] In addition to the KFM measurements we used a balance to record long range electrostatic attraction as a function of separation. The balance (Ohaus Adventurer) was used in combination with a micromanipulator to record force distance curves described later. In the force measurement experiments the contacting structure is mounted onto the plate of a microbalance which records a weight reduction after forced delamination.

Figure 2.2 depicts the KFM images of (a) PMMA versus (b) SiO_2 surfaces after being brought in contact with PDMS and our hypothesis of the charging mechanism. Experimentally we find that PMMA charged positively at contacted areas while SiO_2 charged negatively. Localized electrification is observed after conformal contacts are delaminated. The edge of stamp-contacted region was recorded as well since it is an area where the periodic potential is disturbed. Even this region shows minimal lateral charge diffusion, however no charge patterns are observed in regions where the PDMS did not contact. The uncontacted substrate areas serve as control areas for reference to the charge patterns in the contacted areas. The recorded potential difference in KFM studies can be used as a first order estimate of the trapped surface charge density. In the illustrated example we recorded +250 mV potential difference for the 200 nm thick PMMA film which represents a charge density of 3.25 nC/cm^2 and -300 mV for the 160 nm thick SiO_2 film which represents 7.3 nC/cm^2.[46] The charging could in principle be attributed to a number of factors including material transfer. To determine if material transfer played an important role we conducted several atomic force microscopy (AFM) and x-ray photon spectroscopy (XPS) studies. We found no measurable material transfer between plasma treated PDMS and untreated PMMA which is consistent with prior XPS studies by others.[41-44] Yet PMMA charges highly upon contact. In the case of SiO_2 things are more complicated and are more sensitive to the details of oxygen plasma treatment. We tested two types of plasmas with different oxygen concentrations and pressure. Specifically a 1 minute 100% oxygen plasma treatment at 100 mTorr which is used for etching (STS RIE etcher) was found to lead to covalent bonding between the PDMS and SiO_2 with a detectable amount of PDMS transferred upon forced delamination. Yet these PDMS stamps did not provide the highest level of charge and could not be used repeatedly. In contrast at 10 Torr air based 20% oxygen plasma treatment (SPI Plasma Prep II) for the same time allowed delamination of the PDMS from SiO_2 producing high charge levels and low material transfer. The latter PDMS stamps could be used multiple times to charge a surface as will be discussed in figure 2.3. The lack of correlation between charge and material transfer combined with the ability to support successive charging leads to the conclusion that material transfer is not the dominant charging mechanism.

The working hypothesis for the charging mechanism is illustrated in figure 2.2c and involves hydrogen proton exchange at the interface. It is known that plasma treatment attacks the Si-CH_3 bonds on the surface of the PDMS leaving very reactive silyl radicals that capture O, OH, COOH, and oxygen radicals, forming a mildly acidic and highly polar surface.[41,43] PMMA on the other hand can be considered as being “less acidic” than plasma treated PDMS since it contains fewer surface hydrogen atoms. This creates a chemical potential difference that allows hydrogen protons to transfer during contact. After separation, the hydrogen atoms remain trapped on the PMMA surface leaving these areas positively charged. In accordance with this hydrogen proton exchange reaction theory; silicon dioxide was tested as it should yield the opposite polarity since the oxidized surface of the SiO_2 substrate has an abundance of hydroxyl groups making it “more acidic” than PDMS.

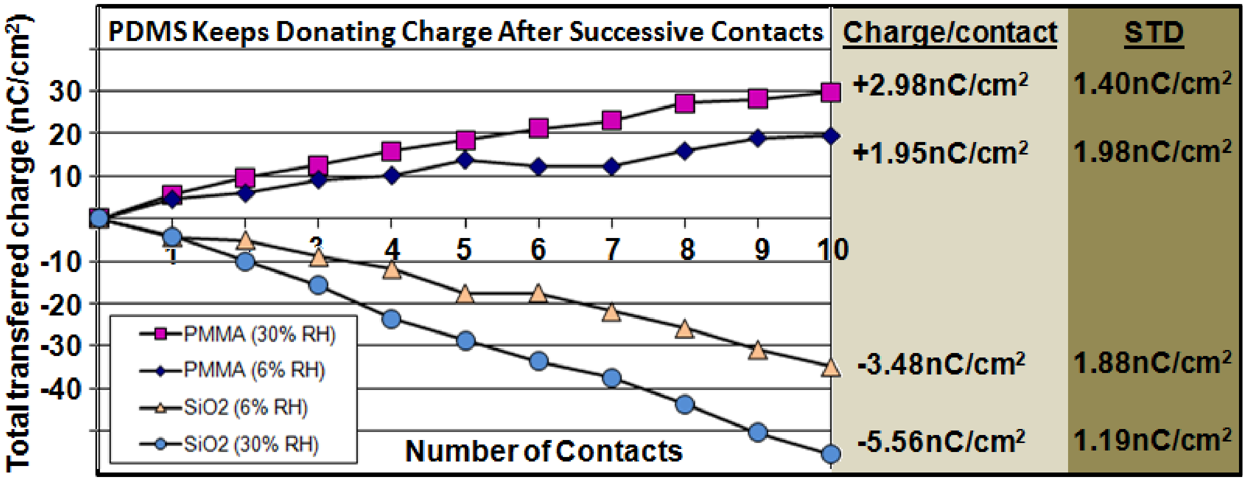

Figure 2.3. Cumulative donated charge from a single piece of PDMS to PMMA and SiO_2 at 6% and 30% relative humidity. Repeated contact to fresh PMMA and SiO_2 surfaces resulted in continued charge transfer. The average charge per contact and standard deviation per contact are displayed next to their respective lines.

In terms of the degradation of the charging ability of the PDMS as a function of use, we found that plasma activated PDMS can be used multiple times before it needs reactivation; no measurable degradation was observed after 10 charging experiments. This observation can be explained if we compare the estimated surface charge densities (3-7 nC/cm^2) with the intermolecular spacing of the reactive sites that are available. 7 nC/cm^2 is a high level of charge which appears to be self-limited by the dielectric breakdown strength of air as will be discussed below. From a molecular standpoint, however, 7 nC/cm^2 is only one elementary charge per 40 nm by 40 nm sized area. For example, the area per silanol group is estimated to be 0.7 nm x 0.7 nm. This leads to an abundance of surface groups on the PDMS that can continue to take part in the reaction. The large quantity of surface groups supports the observation that the PDMS can be used as a charge source multiple times.

2.3 Charging Results and Force Measurements: Figure 2.3 plots the resulting amount of charge that was donated by a single piece of PDMS over successive contacts. The amount of charge that is donated in each step can be monitored by placing each freshly charged sample on a Faraday cup. The Faraday cup is connected to a Keithley 6517A electrometer which records the induced image charge which provides a direct measure of how much charge has been donated to the two dielectrics, PMMA or SiO_2. Each time the same piece of PDMS contacted a fresh dielectric surface. The figure shows PMMA in the upper half and SiO_2 in the lower half. The results show that increasing the humidity from 6% to 30% increased the amount of overall charge transferred. It has previously been reported that water plays an important role in triboelectric charging of toner particles and polymers[47-49] where faster charging was observed[50] at higher relative humidity. A similar trend was observed in a more recent and unrelated study that reported that surface can be charged through gas-surface reactions. The authors changed the relative humidity[51,52] and found higher levels of uncompensated surface charge at raised humidity. In our case the increased charge levels could be explained by the polymeric amorphous and hydrophilic structure of oxygen plasma treated PDMS which leads to a greater uptake of water and ionic species to participate in the ion transfer.

Using the KFM based estimated 3-7 nC/cm^2 of uncompensated surface charge we can evaluate the resulting electric field $\boldsymbol{E=\sigma/\varepsilon_0}$ where $\boldsymbol{\sigma}$ is the surface charge density, and $\boldsymbol{\varepsilon_0}$ is the permittivity of air gap that is formed. The estimated values for the electric field are 3.5 x10^6 V/m for PMMA and 8x10^6 V/m for SiO_2 which exceeds the dielectric breakdown strength of air (~3x10^6 V/m) published for macroscopic electrodes. The closeness of these values to the theoretical limit raises the issue if the observed charge levels are limited or self-regulated by dielectric breakdown strength of air. In principle it could be possible that electrostatic discharge takes place during charge separation which limits the charge level to the reported values. Short range discharge phenomena between separating surfaces have been reported by Horn *et al.*[31] using surface force apparatus measurements; the observed abrupt reductions in the Coulomb attraction were attributed to a stepwise reduction in the remaining uncompensated charges. These types of discharges occur over short distances and may therefore not be accompanied with light flashes and

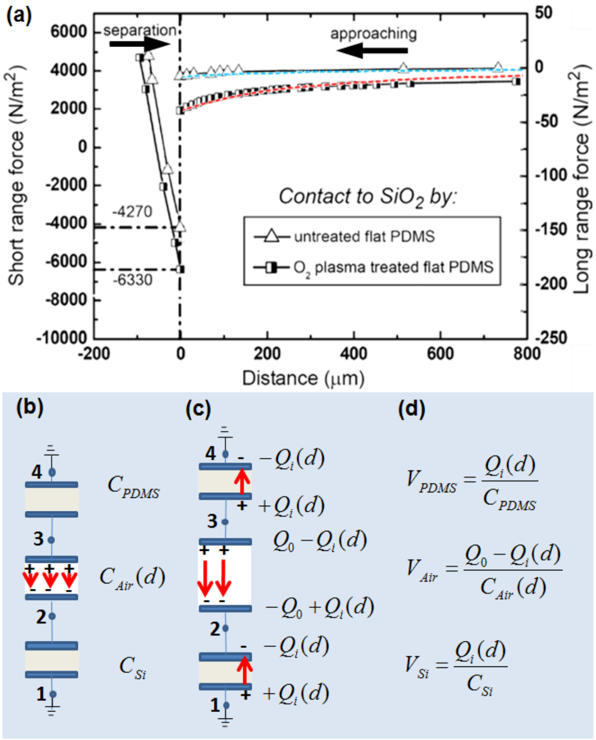

(e) $\sum V=0 \Rightarrow V_{PDMS}+V_{Si}=V_{Air}$ to find:

$$Q_i(d)=\frac{Q_0}{1+C_{Air}\left(\frac{1}{C_{PDMS}}+\frac{1}{C_{Si}}\right)}=\frac{Q_0}{1+\frac{C_{Air}(d)}{C_{Stray}}}$$

(f)

$$F_{Air}=\frac{(Q_0-Q_i(d))^2}{2\cdot d\cdot C_{Air}(d)} \qquad \boxed{\frac{F_{Air}}{A}=\frac{\sigma_0^{\,2}}{2\varepsilon_0}\,\frac{1}{\left(1+\frac{C_{Stray}}{\underbrace{\varepsilon_0 A/d}_{C_{Air}}}\right)^2}}$$

Figure 2.4. The right side depicts the recorded long-range Coulomb attractive force as a function of separation which is fit to a stray capacitance model (dashed lines) that accounts for induced image charges in nearby conductors. (b,c) As the two surfaces are separated $C_{Air}(d)$ is reduced and the field distribution changes to involve the stray capacitance to nearby grounded surfaces, resulting in a separation-dependent electric field and potential distribution. (d-f) Provides the mathematical steps to derive the force distance curve in the given case where the PDMS was mounted onto a grounded copper plate and the electret was a spin coated layer on a grounded Si substrate.

popping sounds that can be detected by simple observation. While discharges may be present and self-limiting they did not result in localized pockets where complete neutralization took place.

A consequence of separated charges at the interface will be an attractive force which can be estimated using $F/A = \sigma^2/2\varepsilon_0$ where A is the contact area. The estimated electrostatic attraction based in KFM data exceeds 100 N/m^2 suggesting that the charged surface could lift ~9 kg/m^2. To directly measure this estimated attraction we mounted the contacting structure on a balance which monitors the produced lift force after separation. Figure 4a shows the force-distance curves which were measured by recording the weight reduction as a function of separation for SiO$_2$ substrates after contact with untreated and oxygen plasma treated PDMS. The reference is untreated PDMS which provides low levels of contact electrification and low Coulomb attraction. The left side of the graph plots the overall adhesive force before separation occurs (no airgap, short range force scale to the left). The right side of the graph plots the attractive Coulomb force as the substrates reapproach the previously contacted PDMS surfaces (with airgap, long range force scale to the right). The required force to pull the two plane-parallel surfaces apart (left) is typically two orders of magnitude larger than the maximum long range attractive force with an airgap in place (right). At present the long range attractive force across an airgap reaches 50 N/m^2 before the two surfaces snap into contact. This is the highest possible data point we have recorded so far. The last data point is difficult to record as it depends on how parallel the surface are when they reapproach each other which may also explain the discrepancy between this ~50 N/m^2 value and the KFM based estimate which predicted >100 N/m^2. However, both KFM and direct force measurements confirm that the values for the charge density, electric field, and forces are near the theoretical limit set by the dielectric breakdown of air.

In our force-distance measurements the PDMS and electret surfaces were mounted on grounded copper plates as depicted schematically in figure 2.4b which act as Faraday cups which provide the ability to monitor image charges. Image charges are a direct result of stray capacitances to nearby conductors and dielectric materials that surround the charged layers. Figure 2.4c shows that any stray capacitance will reduce the measured long-range force of adhesion as the separation is increased. In other words the force is not constant as suggested by the previously discussed equation where the force density $F/A=\sigma^2/2\varepsilon_0$ is independent of separation d. A more accurate model for the force-distance curves can be found following figure 2.4d and 2.4e. The result is shown in figure 4f using $F/A= \sigma^2/2\varepsilon_0 * 1/(1 + C_{stray}/[\varepsilon_0 A/d])^2$ where C_{stray} is related to stray capacitance of the charged surfaces to both grounded copper plates. The model is derived by applying the integral form of Gauss' law around the top and bottom electrodes followed by superposition of the respective electric fields. For the $d=0$ limit case the force reduces to the equation $F/A=\sigma^2/2\varepsilon_0$ discussed earlier to estimate transferred charge densities and the image charges in the nearby copper mounting plates are negligible.

2.4. Nanocontact Electrification Applications:

Figure 2.5 discusses applications of uncompensated surface charges. Figure 2.5a shows an application where the recorded charge pattern (left, KFM image) is used to attract nanoparticles (right, SEM image). In the given example, <50 nm sized negatively charged silver particles were deposited directly from the gas phase using a previously reported nanomaterial source.[38,39] The image demonstrates that the field is strong enough to attract the particles to the charged areas with 200nm resolution.

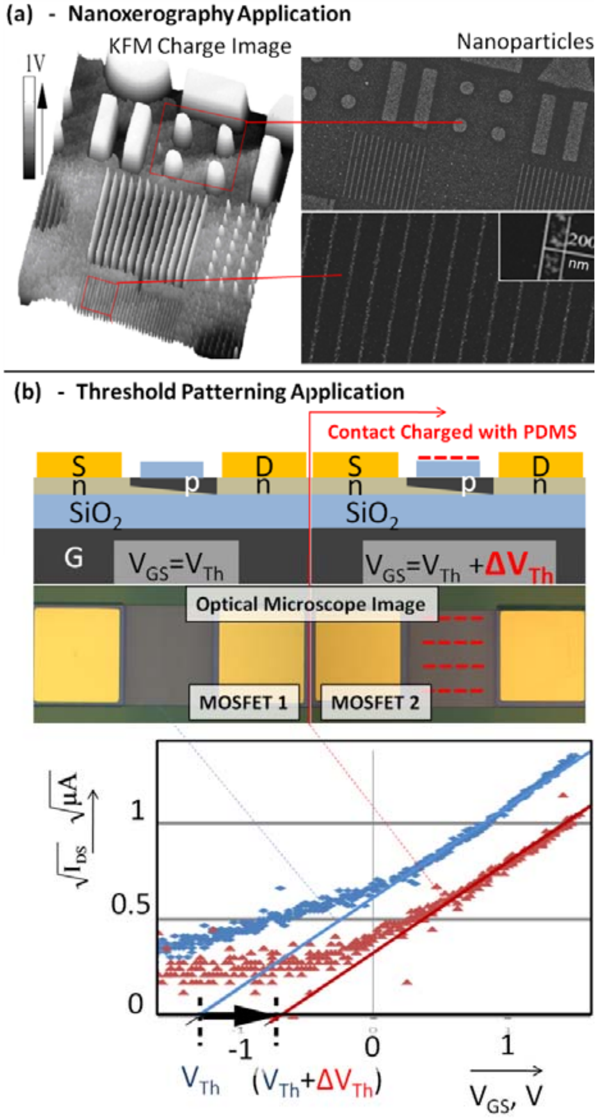

Figure 2.5. Applications of contact electrification in nanoxerography and thin film electronics. (a) KFM charge images and corresponding 200 nm resolution nanoxerography nanoparticle prints. (b) Thin film electronics application showing schematic, optical microscope image, and $\sqrt{I_{DS}}$ vs. V_{GS} plot of charge patterned MOSFETs achieving a threshold voltage shift of 580mV.

Figure 2.5b shows that contact electrification can also be used to alter electronic transport in nearby semiconducting device layers. In the demonstrated application patterning of charge is used to alter the threshold voltage of thin film Si transistors from one area to another. Figure 5b shows a device schematic before (left) and after contact (right); full fabrication details are described in the methods section. The I_{DS} vs. V_{GS} transistor curves shown were taken using the handle wafer as a back gate. We used the x-axis intercept of $\sqrt{I_{DS}}$ vs. V_{GS} line to evaluate the threshold voltage.[53] For SiO_2 the threshold voltage applied to the back gate shifts to a 580mV higher voltage which is consistent with the expected presence of negative surface charge on the SiO_2 surface.

2.5 Conclusion: In conclusion the cleavage of conformal contacts, which has become a common procedure in areas of soft-lithography and other soft-printing processes, typically leaves behind large amounts of surface charge as the surfaces are delaminated. While these surface charges remain undetected with most commonly applied spectroscopic measurement techniques including XPS and FTIR, direct evidence can be gained through Kelvin probe force microscopy and force distance curve measurements. The recorded charging levels can be very high and the upper levels seem to be self-limited by the dielectric breakdown strength of air. The separated charges give rise to an electrostatic force of adhesion that can be detected over millimeter distances, exceeding 50 N/m^2 in some cases. The corresponding force distance curves depict a phenomenological relationship between short and long-range attractive forces. The presented explanation suggests a two-step process whereby the formation and delamination of interfaces bonded by ions precedes contact electrification and the generation of long-range electrostatic forces. SiO_2 and SU-8 are commonly used in the processing of semiconductor devices. We therefore expect that our findings will impact areas which go beyond the demonstrated charge directed assembly and transfer applications. Specifically the emerging field of printable and flexible electronics could be impacted, where contact printing methods and delamination of interfaces are used to print and transfer materials. We anticipate that the presence of high levels of uncompensated charges may alter the functionality of various electronic devices including FETs unless models take these extra gate charges into account. The additional challenges are particularly relevant in the context of flexible electronics where thin semiconductors, polymer insulators, and conformal contacts are widely employed.

3. Acknowledgements: We acknowledge support of this work by NSF CMMI-0755995.

4. References:

[1] Devoret, M. H.and Schoelkopf, R. J., "Amplifying Quantum Signals with the Single-Electron Transistor," Nature, vol. 406, pp. 1039-1046, 2000.

[2] Ding, Y., Dong, Y., Campbell, S. A., Jacobs, H. O., Bapat, A., Kortshagen, U., Perrey, C.and Carter, C. B., "Field-Effect Transistor Built with a Single Crystal Si Nanoparticle," Proceedings of 2005 NSF DMII Grantees Conference, Scottsdale, Arizona,January 3-6, vol. pp. 2005.

[3] Xiang, J., Lu, W., Hu, Y., Wu, Y., Yan, H.and Lieber, C. M., "Ge/Si Nanowire Heterostructures as High-Performance Field-Effect Transistors," Nature (London, United Kingdom), vol. 441, pp. 489-493, 2006.

[4] Fafard, S., Hinzer, K., Raymond, S., Dion, M., Mccaffrey, J., Feng, Y.and Charbonneau, S., "Red-Emitting Semiconductor Quantum Dot Lasers," Science, vol. 274, pp. 1350-1353, 1996.

[5] Patolsky, F., Zheng, G.and Lieber, C. M., "Nanowire-Based Biosensors," Analytical Chemistry, vol. 78, pp. 4260-4269, 2006.

[6] Law, M., Sirbuly, D. J., Johnson, J. C., Goldberger, J., Saykally, R. J.and Yang, P., "Nanoribbon Waveguides for Subwavelength Photonics Integration," Science (Washington, DC, United States), vol. 305, pp. 1269-1273, 2004.

[7] Brune, H., Giovannini, M., Bromann, K.and Kern, K., "Self-Organized Growth of Nanostructure Arrays on Strain-Relief Patterns," Nature, vol. 394, pp. 451-453, 1998.

[8] Xia, Y., Yin, Y., Lu, Y.and Mclellan, J., "Template-Assisted Self-Assembly of Spherical Colloids into Complex and Controllable Structures," Advanced Functional Materials, vol. 13, pp. 907-918, 2003.

[9] Cui, Y., Bjoerk, M. T., Liddle, J. A., Soennichsen, C., Boussert, B.and Alivisatos, A. P., "Integration of Colloidal Nanocrystals into Lithographically Patterned Devices," Nano Letters, vol. 4, pp. 1093-1098, 2004.

[10] Kimura, K., Yao, H.and Sato, S., "Self-Assembling of Gold and Silver Nanoparticles at a Hydrophilic/Hydrophobic Interface: A Synthetic Aspect and Superstructure Formation," Synthesis and Reactivity in Inorganic, Metal-Organic, and Nano-Metal Chemistry, vol. 36, pp. 237-264, 2006.

[11] Yellen, B. B.and Friedman, G., "Programmable Assembly of Heterogeneous Colloidal Particle Arrays," Advanced Materials, vol. 16, pp. 111-115, 2004.

[12] Li, D., Ouyang, G., Mccann, J. T.and Xia, Y., "Collecting Electrospun Nanofibers with Patterned Electrodes," Nano Letters, vol. 5, pp. 913-916, 2005.

[13] Duan, X., Huang, Y., Cui, Y., Wang, J.and Lieber, C. M., "Indium Phosphide Nanowires as Building Blocks for Nanoscale Electronic and Optoelectronic Devices," Nature (London), vol. 409, pp. 66-69, 2001.

[14] Jacobs, H. O.and Barry, C. US Patent 2004-982179 2005123687, 2005.

[15] Jacobs, H. O.and Whitesides, G. M., "Submicrometer Patterning of Charge in Thin-Film Electrets," Science, vol. 291, pp. 1763-1766, 2001.

[16] Barry, C. R., Lwin, N. Z., Zheng, W.and Jacobs, H. O., "Printing Nanoparticle Building Blocks from the Gas Phase Using Nanoxerography," Applied Physics Letters, vol. 83, pp. 5527-5529, 2003.

[17] Barry, C. R., Gu, J.and Jacobs, H. O., "Charging Process and Coulomb-Force-Directed Printing of Nanoparticles with Sub-100-Nm Lateral Resolution," Nano Letters, vol. 5, pp. 2078-2084, 2005.

[18] Krinke, T. J., Fissan, H., Deppert, K., Magnusson, M. H.and Samuelson, L., "Positioning of Nanometer-Sized Particles on Flat Surfaces by Direct Deposition from the Gas Phase," Applied Physics Letters, vol. 78, pp. 3708-3710, 2001.

[19] Mesquida, P.and Stemmer, A., "Attaching Silica Nanoparticles from Suspension onto Surface Charge Patterns Generated by a Conductive Atomic Force Microscope Tip," Advanced Materials (Weinheim, Germany), vol. 13, pp. 1395-1398, 2001.

[20] Naujoks, N.and Stemmer, A., "Micro- and Nanoxerography in Liquids - Controlling Pattern Definition," Microelectronic Engineering, vol. 78-79, pp. 331-337, 2005.

[21] Fudouzi, H., Kobayashi, M.and Shinya, N., "Assembling 100 Nm Scale Particles by an Electrostatic Potential Field," Journal of Nanoparticle Research, vol. 3, pp. 193-200, 2001.

[22] Welle, A. M.and Jacobs, H. O., "Printing of Organic and Inorganic Nanomaterials Using Electrospray Ionization and Coulomb-Force-Directed Assembly," Applied Physics Letters, vol. 87, pp. 263119, 2005.

[23] Bapat, A., Perrey, C. R., Campbell, S. A., Carter, C. B.and Kortshagen, U., "Synthesis of Highly Oriented, Single-Crystal Silicon Nanoparticles in a Low-Pressure, Inductively Coupled Plasma," J. Appl. Phys., vol. 94, pp. 1969-1974, 2003.

[24] Jacobs, H. O.and Stemmer, A., "Measuring and Modifying the Electric Surface Potential Distribution on a Nanometre Scale: A Powerful Tool in Science and Technology," Surface & Interface Analysis, vol. 27, pp. 361-367, 1999.

[25] Jacobs, H. O., Knapp, H. F., Muller, S.and Stemmer, A., "Surface Potential Mapping - a Qualitative Material Contrast in Spm," Ultramicroscopy, vol. 69, pp. 39-49, 1997.

[26] Whitby, K. T., "Generator for Producing High Concentrations of Small Ions," Review of Scientific Instruments, vol. 32, pp. 1351-5, 1961.

[27] Romay, F. J., Liu, B. Y. H.and Pui, D. Y. H., "A Sonic Jet Corona Ionizer for Electrostatic Discharge and Aerosol Neutralization," Aerosol Science and Technology, vol. 20, pp. 31-41, 1994.

[28] Dong, Y., Bapat, A., Hilchie, S., Kortshagen, U.and Campbell, S. A., "The Generation of Free-Standing Single Crystal Silicon Nanoparticles," J. Vac. Sci. and Technol. B, vol. 44, pp. 1923-30, 2004.

[29] Barry, C. R., Steward, M. G., Lwin, N. Z.and Jacobs, H. O., "Printing Nanoparticles from the Liquid and Gas Phases Using Nanoxerography," Nanotechnology, vol. 14, pp. 1057-1063, 2003.

[30] Barry, C. R., Lwin, N. Z., Zheng, W.and Jacobs, H. O., "Printing Nanoparticle Building Blocks from the Gas-Phase Using Nanoxerography," Appl. Phys. Lett., vol. 83, pp. 5527, 2003.

[31] Horn, R., Smith, D.and Grabbe, A., "Contact Electrification Induced by Monolayer Modification of a Surface and Relation to Acid-Base Interactions," Nature, vol. 366, pp. 442-3, 1993.

[32] Xia, Y.and Whitesides, G., "Soft Lithography," Annu. Rev. Mater. Sci., vol. 28, pp. 153-184, 1998.

[33] Loo, Y., Willett, R., Baldwin, K.and Rogers, J., "Interfacial Chemistries for Nanoscale Transfer Printing," J. Am. Chem. Soc., vol. 124, pp. 7654-7655, 2002.

[34] Jacobs, H.and Whitesides, G., "Submicrometer Patterning of Charge in Thin-Film Electrets," Science, vol. 291, pp. 1763-1766, 2001.

[35] Fudouzi, H., Kobayashi, M.and Shinya, N., "Site-Controlled Deposition of Microsized Particles Using an Electrostatic Assembly," Advanced Materials, vol. 14, pp. 1649-1652, 2002.

[36] Liang, S., Chen, M., Xue, Q.and Liu, Z., "Micro-Patterning of Tio2 Thin Films by Photovoltaic Effect on Silicon Substrates," Thin Solid Films, vol. 516, pp. 3058-3061, 2008.

[37] Park, J.-U., Lee, S., Unarunotai, S., Sun, Y., Dunham, S., Song, T., Ferreira, P. M., Alleyene, A. G., Paik, U.and Rogers, J. A., "Nanoscale, Electrified Liquid Jets for High-Resolution Printing of Charge," Nano Letters, vol. 10, pp. 584-591, 2010.

[38] Barry, C., Steward, M., Lwin, N.and Jacobs, H., "Printing Nanoparticles from the Liquid and Gas Phases Using Nanoxerography," Nanotechnology, vol. 14, pp. 1057-1063, 2003.

[39] Barry, C., Lwin, N., Zheng, W.and Jacobs, H., "Printing Nanoparticle Building Blocks from the Gas-Phase Using Nanoxerography," Appl. Phys. Lett., vol. 83, pp. 5527, 2003.

[40] Barry, C., Gu, J.and Jacobs, H., "Charging Process and Coulomb-Force-Directed Printing of Nanoparticles with Sub-100-Nm Lateral Resolution," Nano Lett., vol. 5, pp. 2078-2084, 2005.

[41] Youn, B.and Huh, C., "Surface Analysis of Plasma-Treated Polydimethylsiloxane by X-Ray Photoelectron Spectroscopy and Surface Voltage Decay," Surf. Interface Anal., vol. 35, pp. 445-449, 2003.

[42] Kim, H., Cho, Y., Lee, H., Kim, S., Ryu, S., Kim, D., Kang, T.and Chung, K., "High-Brightness Light Emitting Diodes Using Dislocation-Free Indium Gallium Nitride/Gallium Nitride Multiquantum-Well Nanorod Arrays," Nano Lett., vol. 4, pp. 1059-1062, 2004.

[43] Bhattacharya, S., Datta, A., Berg, J.and Gangopadhyay, S., "Studies on Surface Wettability of Poly(Dimethyl) Siloxane (Pdms) and Glass under Oxygen-Plasma Treatment and Correlation with Bond Strength," J. Microelectromech. S., vol. 14, pp. 590-597, 2005.

[44] Langowski, B.and Uhrich, K., "Oxygen Plasma-Treatment Effects on Si Transfer," Langmuir, vol. 21, pp. 6366-6372, 2005.

[45] Jacobs, H., Knapp, H., Muller, S.and Stemmer, A., "Surface Potential Mapping - a Qualitative Material Contrast in Spm," Ultramicroscopy, vol. 69, pp. 39-49, 1997.

[46] Sugunan, A., Warad, H. C., Boman, M.and Dutta, J., "Zinc Oxide Nanowires in Chemical Bath on Seeded Substrates: Role of Hexamine," J. Sol-Gel Sci. and Tech., vol. 39, pp. 49-56, 2006.

[47] Nomura, T., Satoh, T.and Masuda, H., "The Environment Humidity Effect on the Tribo-Charge of Powder," Powder Technology, vol. 135-136, pp. 43-49, 2003.

[48] Nemeth, E., Albrecht, V., Schubert, G.and Simon, F., "Polymer Tribo-Electric Charging: Dependence on Thermodynamic Surface Properties and Relative Humidity," Journal of Electrostatics, vol. 58, pp. 3-16, 2003.

[49] Albrecht, V., Janke, A., Nemeth, E., Spange, S., Schubert, G.and Simon, F., "Some Aspects of the Polymers' Electrostatic Charging Effects," Journal of Electrostatics, vol. 67, pp. 7-11, 2009.

[50] Gouveia, R. F., Costa, C. A. R.and Galembeck, F., "Water Vapor Adsorption Effect on Silica Surface Electrostatic Patterning," Journal of Physical Chemistry C, vol. 112, pp. 17193-17199, 2008.

[51] Gouveia, R. F.and Galembeck, F., "Electrostatic Charging of Hydrophilic Particles Due to Water Adsorption," Journal of the American Chemical Society, vol. 131, pp. 11381-11386, 2009.

[52] Ducati, T. R. D., Simoes, L. H.and Galembeck, F., "Charge Partitioning at Gas-Solid Interfaces: Humidity Causes Electricity Buildup on Metals," Langmuir, vol. 26, pp. 13763-13766, 2010.

[53] Wainright, S. P., Hall, S.and Flandre, D., "The Effect of Series Resistance on Threshold Voltage Measurement Techniques for Fully Depleted Soi Mosfets," Solid State Electron., vol. 39, pp. 89-94, 1996.